A phase synthesis time reversal impact imaging method for on-line composite structure monitoring

Lei Qiu and Shenfang Yuan*

The Aeronautic Key Lab for Smart Materials and Structures, Nanjing University of Aeronautics and Astronautics, Nanjing, P.R China

Abstract. Comparing to active damage monitoring, impact localization on composite by using time reversal focusing method has several difficulties. First, the transfer function of the actuator-sensor path is difficult to be obtained because of the limitation that no impact experiment is permitted to perform on the real structure and the difficulty to model it because the performance of real aircraft composite is much more complicated comparing to metal structure. Second, the position of impact is unknown and can not be controlled as the excitation signal used in the active monitoring. This makes it not applicable to compare the difference between the excitation and the focused signal. Another difficulty is that impact signal is frequency broadband, giving rise to the difficulty to process virtual synthesis because of the highly dispersion nature of frequency broadband Lamb wave in plate-like structure. Aiming at developing a practical method for on-line localization of impact on aircraft composite structure which can take advantage of time reversal focusing and does not rely on the transfer function, a PZT sensor array based phase synthesis time reversal impact imaging method is proposed. The complex Shannon wavelet transform is presented to extract the frequency narrow-band signals from the impact responded signals of PZT sensors. A phase synthesis process of the frequency narrow-band signals is implemented to search the time reversal focusing position on the structure which represents the impact position. Evaluation experiments on a carbon fiber composite structure show that the proposed method realizes the impact imaging and localization with an error less than 1.5 cm. Discussion of the influence of velocity errors and measurement noise is also given in detail.

Keywords: structural health monitoring; time reversal; phase synthesis; impact imaging; composite structure; complex Shannon wavelet transform.

1. Introduction

Advanced composites are increasingly used on aircraft where weight and performance are a great concern. Composites are very sensitive to impact which can cause inner damages in the composite, such as delamination. These relatively small inner damages usually are difficult to be found by routine inspections. However the structural integrity may be significantly degraded. Impact may happen during the whole service life of the aircraft structure from manufacturing process to the whole service life. Early detection and on-line monitoring of impact position can greatly help to prevent catastrophic failure and reduce the ground maintenance time of aircraft.

Many investigations have been reported regarding localization methods of impact. Among them,

---

*Corresponding Author, Professor, E-mail: ysf@nuaa.edu.cn

one branch of typical methods is based on the time-of-arrival of impact signals. These methods often suffer from the difficulty of setting threshold to decide the exact time-of-flight of the acoustic signal caused by impact because of signal noise and scatters caused by rivets, holes and stiffeners in complex structures (Coverley and Staszewski 2003, Meo *et al*. 2005, Efstratios and Evangelos 2007, Kundu *et al*. 2008, Staszewski *et al*. 2009). Another kind of method uses pattern recognition models, such as neural networks. These methods usually have to obtain training data first from the structure to build feature libraries and use them to train the pattern recognition models before the methods real start to work (Jones *et al*. 1995, Staszewski and Worden 2000, Haywood *et al*. 2005). Because different structures usually have differences in their performances, in practical application, models trained by certain structures are not easy to be applied on other structures. For some special materials, such as composite, no beforehand impact experiments are permitted to be done to obtain the training data on the structures which are needed to be monitored because even the experimental impacts may cause damages in the structure. These factors limit the application of the above methods. Some researches were performed based on mechanical models (Shin 2000, Inoue *et al*. 2001, Hu and Fukunaga 2007). Since the accurate mechanical models of structures are difficult to be obtained, especially composite, the practical applications usually meet many difficulties. A better method to realize the impact localization on composite structure should be a method which does not need modeling of the structure and is of a promising precision.

Recently, several researchers reported their contributions in localization the impact position taking advantages of the time reversal focusing methods (Ing *et al*. 2005, Ribay *et al*. 2007, Chen and Yuan 2010, Meo and Ciampa 2011). Most of these researches were done on metal structure or glass plate. Only Meo *et al*. reported the research on composite structure (Meo and Ciampa 2011). In fact, many attentions have been paid to the research of time reversal focusing method in recent years in structural health monitoring especially in active Lamb wave based damage monitoring because this method has shown a promising advantage to give a focusing image of the structural damage and can improve the signal-to-noise ratio of the propagating waves (Fink 1992, 1999, Ing and Fink 1996, 1998, Prada and Fink 1998, Wang *et al*. 2004, Xu and Giurgiutiu 2007, Park *et al*. 2007, 2009). In these literatures, PZT arrays are usually adopted. After exciting the structure using one of the PZT elements, responses received by other PZT elements are time reversed and applied back to each corresponding PZT element respectively. It has been proved that these signals are focused at the position of the excitation point. By comparing the focused signal and the original excitation signal at the excitation position, difference between signals can be used to identify the damage in the structure. Since re-exciting each PZT elements needs complicated hardware to support, some researchers conducted further researches to use software realization of the time reversal focusing process. To do this, transfer functions of the propagation of the signals on structure are obtained first and stored in computer, and virtual realization based on the transfer functions of the time reversal focusing process is conducted in software (Wang and Yuan 2005, Ing *et al*. 2005, Ribay *et al*. 2007, Chen and Yuan 2010, Cai *et al*. 2011, Meo and Ciampa 2011). A key issue in these methods is to obtain the transfer functions of the wave propagation between excitation element and the sensing element. Usually three typical methods are used to obtain the transfer functions: (1) mechanical modeling of the structure (Wang and Yuan 2005); (2) finite element modeling of the structure (Chen and Yuan 2010); (3) measuring the transfer functions through experiments (Ing *et al*. 2005, Ribay *et al*. 2007, Cai *et al*. 2011, Meo and Ciampa 2011).

Comparing to active damage monitoring by using time reversal focusing method, impact localization

on composite has several difficulties. First, impact localization is a passive process. The position of impact is totally unknown and can not be controlled as the excitation signal used in the active damage monitoring method which both position and excitation waveforms can be controlled. This makes it not applicable to compare the difference between the excitation and the focused signal. Different from the ordinary frequency narrow-band excitation signal used in the active method, impact signal is frequency broadband. Since the dispersion nature of different Lamb wave modes in plate-like structure, the signal has a wide range of frequency components which are of different propagation velocities causing it difficult to process virtual synthesis. Second, the real aircraft composite usually has a more complicated performance giving rise to the difficulty to be modeled comparing to the ordinary metal structure. A practical method should not rely on the modeling. Another important limitation on composite is that no impact experiment is permitted to perform on the real structure because the impact experiment itself may cause damage in the structure.

Though Meo and Ciampa reported their work regarding impact localization on composite structure, they only use one pair of sensor and actuator which can not take advantage of the focusing ability of the time reversal method (Meo and Ciampa 2011). What is important, in their research they still adopted the ordinary experimental transfer function obtaining method. They used hammer to perform impact experiments on the structure first. Because of the anisotropic feature of the composite, they divided the structure into many small intervals and did impact experiments at each "observation points" to obtain the transfer functions at different directions. As mentioned above, for real applications of the impact localization method on aircraft composite structure, this method is not permitted. Narrow-band acoustic emission sensor is adopted in their research to extract narrow band signal from the wide band acoustic signal for time reversal. It works. But considering the real application of structural health monitoring on aircraft, both active damage monitoring and impact passive monitoring are needed. The monitoring system should not apply high weight to the aircraft. Using one system to realize both functions is a promising way. Since PZT sensors are the typical sensors used in the active monitoring system, an impact method based on PZT sensor is a better choice.

In this paper, aiming at developing a practical method for on-line localization of impact on aircraft composite structure which can take advantage of the time reversal focusing method, a PZT sensor array based phase synthesis time reversal impact imaging method for on-line composite structure monitoring is proposed. In this method, frequency narrow-band signals are extracted from impact responded signals of PZT sensors. A phase synthesis process is implemented to search the time reversal focusing position in impact monitoring area which represents the impact position. An imaging representing method is using in the paper to show the searching results. From this image, the impact position can be estimated directly.

Detail methods are introduced in following sections. Section 2 introduces the basic theory of the PZT sensor array based impact imaging method using phase synthesis time reversal focusing for composites. In order to realize the phase synthesis and don't rely on modeling or transfer function, the complex Shannon wavelet transform based frequency narrow-band signal extraction method is presented and also used to obtain the group velocity of the extracted frequency narrow-band signals. Detail descriptions are included in section 3. Evaluation researches are introduced in section 4 which are performed on a carbon fiber composite specimen. Detail discussions of the evaluation results are also given in this section.

2. Impact imaging method using phase synthesis time reversal focusing

According to the time reversal focusing concept, a signal can be focused at the original excitation point if some sensed signals recorded at different points are reversed in the time domain and re-emitted back to the original source point. This time reversibility is based on the spatial reciprocity and time-reversal invariance of linear wave equations (Fink 1992). Fig. 1 shows the time reversal focusing process. $E_C(\omega)$ is the signal excited at the original source. H_{Ci} is the frequency response of transfer function of the signal propagating from C to the PZT i. The output sensing signal of the PZT i can be represented as

$$E_i(\omega) = H_{Ci}(\omega, r)E_C(\omega) \tag{1}$$

When the sensed signal of each PZT sensor is time reversed and re-emitted back to the original source position. A synthesis signal at the source C is obtained by

$$E_C'(\omega) = \sum_{i=1}^{n} H_{Ci}(\omega, r)E_i(\omega)^* \tag{2}$$

where the superscript '*' denotes complex conjugate. It means in the frequency domain, time reversal of a signal is equivalent to phase conjugation (Wang *et al.* 2004). According to the spatial reciprocity of linear wave equation, there is $H_{iC} = H_{Ci}$. By substituting Eq. (1) into Eq. (2), the synthesis signal at C can be represented as

$$E_C'(\omega) = (\boldsymbol{H}(\omega, r)\boldsymbol{H}(\omega, r)^*)E_C(\omega)^* = |\boldsymbol{H}(\omega)|^2 E_C(\omega)^* \tag{3}$$

where $\boldsymbol{H}(\omega, r)$ is the transfer functions matrix of the signals. The term of $|\boldsymbol{H}(\omega, r)|^2$ is a real positive even function. Depending on the basic time reversal theory of Lamb wave propagating on plate-like structure, the modulus value of the synthesis signal reaches the maximum at the position C because all the time reversed signals arrive at the source point at the same time and add together because of the spatial reciprocity and time-reversal invariance of linear wave equations (Wang *et al.* 2004, Núñez and Negreira 2005, Park *et al.* 2007, 2009).

To a frequency narrow-band Lamb wave signal at low frequency, only A_0 mode and S_0 mode exist and the amplitude of A_0 mode is much higher than that of S_0 mode. Thus, the Lamb wave can be considered to be a frequency narrow-band single-mode Lamb wave (Xu and Giurgiutiu 2007) and the transfer function $H(\omega, r)$ can be simplified to
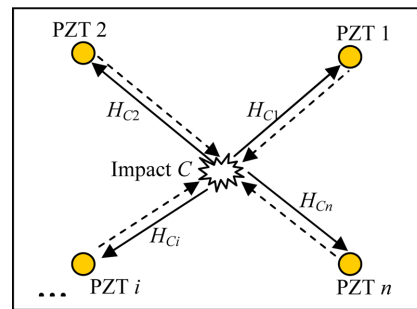

Fig. 1 Illustration of time reversal focusing process of impact signals

$$H(\omega, r) \approx a_{A_0}(\omega, r)e^{-jk_{A_0}(\omega)r} \tag{4}$$

where $a_{A_0}(\omega, r)$ and $k_{A_0}(\omega)r$ are the amplitude term and the phase term of the transfer function, respectively. $k_{A_0}(\omega)$ denotes the wave number of A_0 mode. $k_{A_0}\omega/C_{A_0}$. C_{A_0} denotes phase velocity of A_0 mode. By substituting Eq. (4) into Eq. (3), the synthesis signal at the position C can be changed to

$$E_C^{'}(\omega) = (\boldsymbol{H}(\omega, r)\boldsymbol{H}(\omega, r)^{*})E_C(\omega)^{*} = \sum_{i=1}^{n} |a_{A_0}(\omega, r_{iC})|^2 E_C(\omega)^{*} \tag{5}$$

where the distance from C to all the PZT sensors are denoted as r_{iC}, $i = 1,2,...,n$.

Using Eq. (5), if the transfer functions of A_0 mode can be obtained beforehand, the time reversal focusing process can be realized in software. This is the ordinary software based virtual time reversal method mentioned in section 1.

Regarding the impact imaging of composite material, to apply above method, two difficulties must be solved. First, broadband frequency Lamb wave signals induced by impact have to be processed. Frequency narrow-band signal has to be extracted. Second, the transfer functions of A_0 mode of composite material are difficult to obtain. A method not to rely on the transfer functions should be presented. How to solve the first problem is discussed in detail in next section. A phase synthesis method is put forward to solve the second problem in this section.

Impact position can be also regarded as the signal source C in Fig. 1. Eq. (5) is also applicable when the frequency narrow-band signals have been extracted from the responded signals of the PZT sensors.

The transfer functions shown in Eq. (4) have two terms, the amplitude term and the phase term. Base on the time reversal theory, the two terms have different influence on the focusing results. When the time reversed signals travel back to the source, they arrive at the source at the same time (the same phase) which produces the focusing effect of the time reversal method. This can be proved by Eq. (5) because the focusing signal has nothing to do with the phase term of the transfer functions. On the other hand, the focusing signal has the same shape with the original source signal if the time reversed signals travel back just with the same amplitude term of the transfer functions as that they are emitted out from the source. Regarding the impact imaging, what is concerned is the position of the impact. It is not necessary to obtain a signal synthesized with the same shape as the original signal. In this case, the amplitude term of the transfer function becomes not important. If a virtual synthesis is realized just according to the phase term of the transfer function neglecting the amplitude term, the time reversed signal will still arrive at the source with the same phase, the focusing effect will still happen though the shape of the focusing signal will change and no longer has the same shape with the original signal. This means at the source point, still a maximum amplitude focusing signal will be formed which still can indicate the impact position. This method can be called a phase synthesis method. Instead of transfer functions, this method just needs its phase term which can be calculated from the phase velocity of the A_0 mode when single mode Lamb wave is considered.

To introduce the proposed phase synthesis time reversal focusing and imaging method in more detail, a plate-like structure with n PZT sensors arranged is adopted as an example to explain the method shown in Fig. 2.

In the impact monitoring area, a random position D is chosen whose coordinate is (x, y). The distances from the position D to all the PZT sensors are denoted as $r_1, r_2,..., r_n$. $E_i(\omega)$ is the
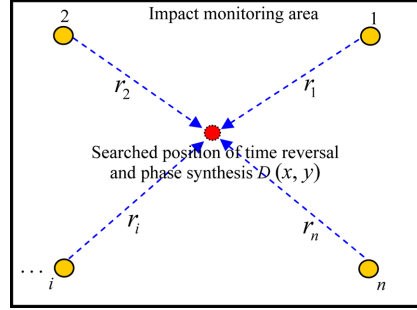
Fig. 2 Schematic diagram of phase synthesis process

frequency response of the frequency narrow-band signal extracted from the impact responded signal of the PZT i. The output synthesis signal at the position D can be represented as Eq. (6) by time reversing $E_i(\omega)$ and applying the phase term of the transfer function $e^{jk_{A_0}(-r_i)}$ to $E_i(\omega)$ at the same time.

$$V_S = \sum_{i=1}^{n} E_i(\omega)^* e^{-jk_{A_0}(\omega)r_i} \tag{6}$$

The modulus value of the inverse Fourier transform of Eq. (6) can be represented as

$$|v_s(t)| = \left| \frac{1}{2\pi} \sum_{i=1}^{n} \int_{-\infty}^{+\infty} E_i(\omega)^* e^{-jk_{A_0}(\omega)r_i} e^{j\omega t} d\omega \right| \tag{7}$$

where $v_s(t)$ denotes the phase synthesis signal. The phase delay factor $e^{-jk_{A_0}(\omega)r_i}$ in Eq. (6) can be represented as

$$e^{-jk_{A_0}(\omega)r_i} = e^{-jr_i\omega/C_{A_0}} \tag{8}$$

Considering that the $E_i(\omega)$ is frequency narrow-band, Eq. (7) can be changed to

$$|v_s(t)| = \left| \frac{1}{2\pi} \sum_{i=1}^{n} \int_{-\infty}^{+\infty} \left(\sum_{\omega_0 \in [\omega_l, \omega_h]} E_i(\omega_0)^* e^{-jr_i\omega_0/C_{\omega_0 A_0}} \right) e^{j\omega t} d\omega \right| = \frac{1}{2\pi} \sum_{i=1}^{n} \left[\sum_{\omega \in [\omega_l, \omega_h]} e_i'\left(\tau - t - r_i/C_{\omega_0 A_0}\right) \right] \tag{9}$$

where $E_i(\omega_0)$ is a frequency component of $E_i(\omega)$ when the frequency is ω_0. $e_i(t)$ is the corresponding time domain signal. $C_{\omega_0 A_0}$ denotes the phase velocity of the frequency component. The ω_0 is in the frequency range of $[\omega_l, \omega_h]$. The frequency band is defined as $\omega_b = \omega_h - \omega_l$ and the center frequency is ω_c.

When imaging the results, the pixel value corresponding to position D is calculated by Eq.(9) representing the modulus value of the focusing signal at position D. It is known that the real focusing only happened at the original source which means here the impact position. The pixel value calculated only at the impact position is the highest. Thus, the whole monitored area can be divided into many small areas, by a searching algorithm to calculate the pixel value of each of these small areas, the impact position can be decided by choosing the highest pixel value position or higher pixel value area.

Since the phase velocities of signals at different frequencies are different, combining with that for composite structure, the phase velocities of waves propagating at different directions are also different, in the searching process, if the phase velocities of different frequencies and propagation

directions are used directly, a large amount of calculation has to be performed. To avoid this, some simplification and approximation are made to solve this problem.

Depending on the dispersion nature of Lamb wave and the superposition principle, the frequency narrow-band Lamb wave can be considered to be consisted of a finite numbers of sine waves. Thus, Eq. (9) can be represented as Eq. (10) approximately

$$\left| v_s(t) \right| \approx \left| \sum_{i=1}^{n} e_i \left(\tau - t + \frac{r_i}{C_{gA_0}} \right) \right| \tag{10}$$

where e_i denotes the frequency narrow-band signal extracted from the impact responded signal of the PZT sensor i.

In this paper, the phase synthesis process is realized in time domain by using group velocity of the frequency narrow-band signals at the center frequency ω_c. Eq. (10) can be changed to the final expression of the phase synthesis signal by using the positive envelope of the frequency narrow-band signals

$$\left| v_s'(t) \right| = \sum_{i=1}^{n} Envelope \left(e_i \left(\tau - t + \frac{r_i}{C_{gA_0}} \right) \right) \tag{11}$$

where *Envelope* denotes the positive envelope. Using this approximation, only the group velocity of the frequency narrow-band signals at the center frequency ω_c is needed. The amount of calculation in the searching process is greatly reduced.

The implementation process of the PZT sensor array based phase synthesis time reversal impact imaging method is shown in Fig. 3.

3. Frequency narrow-band signal extracting and group velocity calculation method

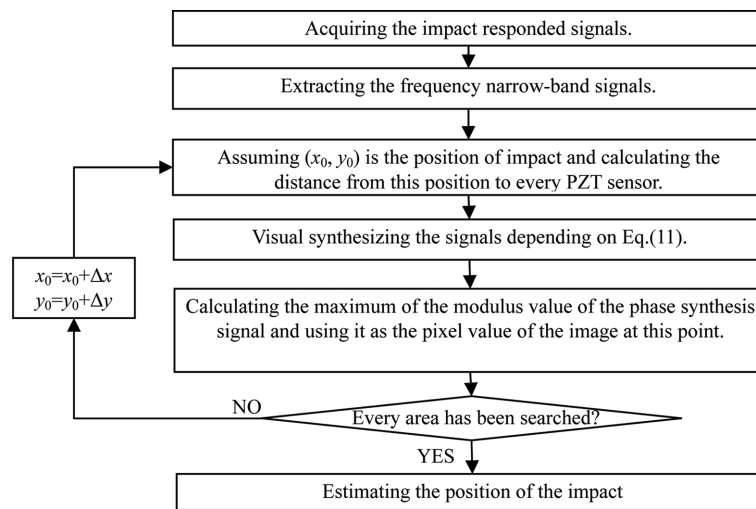In this section, a software processing method based on continuous complex wavelet transform is

Fig. 3 Implementation process of the impact imaging method

proposed taking advantage of its high time-frequency resolution to extract the frequency narrow-band signal corresponding to the A_0 mode of Lamb wave. Different from ordinary wavelet basis function, the frequency response of the complex Shannon wavelet function is a kind of frequency square window which can be used as a good filter to extract a frequency narrow-band signal with the same amplitude sensitivity in the window (Newland 1994, Teolis 1998, Spanos and Kougioumtzoglou 2011).

Eq. (12) shows the complex Shannon wavelet function adopted

$$\Psi(t) = \sqrt{f_b} sinc(f_b t)e^{2\pi i f_c t} \tag{12}$$

The terms of f_b and f_c are the frequency band and center frequency of the wavelet, respectively. The function of *sinc* is represented as

$$sinc(x) = \begin{cases} 1 & x = 0 \\ \dfrac{sin(\pi x)}{\pi x} & x \neq 0 \end{cases} \tag{13}$$

The Fourier transform of Eq. (12) can be represented as:

$$\Phi(\omega) = \begin{cases} \sqrt{\dfrac{2\pi}{\omega_b}} & \omega_c - \dfrac{\omega_b}{2} < \omega \leq \omega_c + \dfrac{\omega_b}{2} \\ 0 & \text{Others} \end{cases} \tag{14}$$

where $\omega_b = 2\pi f_b$, $\omega_c = 2\pi f_c$, $\omega_c = \omega_b/2$. Fig. 4 gives out the real part of complex Shannon wavelet function in different center frequency, frequency band and time factor and their theoretical frequency responses. It indicates that the frequency response of complex Shannon wavelet function is a kind of frequency square window. The width of the window depends on the center frequency and frequency band. Eq. (12) indicates that the center time of complex Shannon wavelet function is at $t = 0$. The center frequency according to Eq. (14) is at $\omega = \omega_c$. The frequency band is limited in the range of (ω_c-$\omega_b/2$, ω_c+$\omega_b/2$]. Therefore, the center time of complex Shannon wavelet transform $\Psi((t-b)/a)$ is at $t = b$. The center frequency is at $\omega = \omega_c/a$. The complex Shannon wavelet transform of the signal $x(t)$ is a frequency narrow-band signal which represents the time-frequency components at $t = b$, $\omega = \omega_c/a$ and the frequency band is $\left(\dfrac{\omega_c}{a} - \dfrac{\omega_b}{2a}, \dfrac{\omega_c}{a} + \dfrac{\omega_b}{2a} \right]$.

(a) Real part of the complex Shannon wavelet functions　　(b) Theoretic Frequency responses
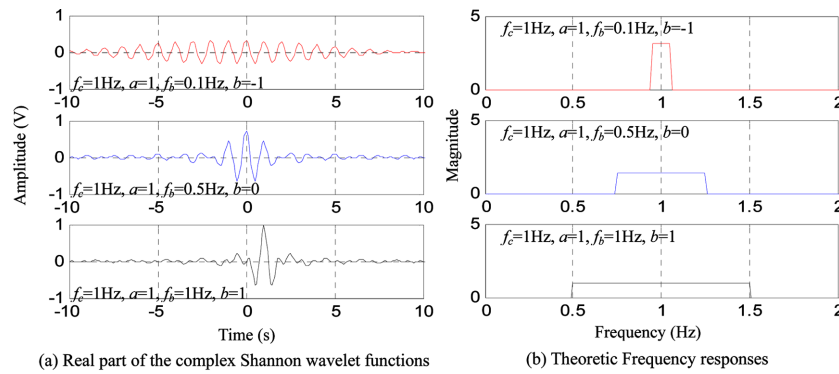
Fig. 4 Real part waveforms and theory frequency responses of the complex Shannon wavelet functions

(a) Impact responded signal

(b) Frequency response of the impact responded signal

Fig. 5 Impact responded signal and the frequency response

(a) Real part of the frequency narrow-band signal

(b) Frequency response

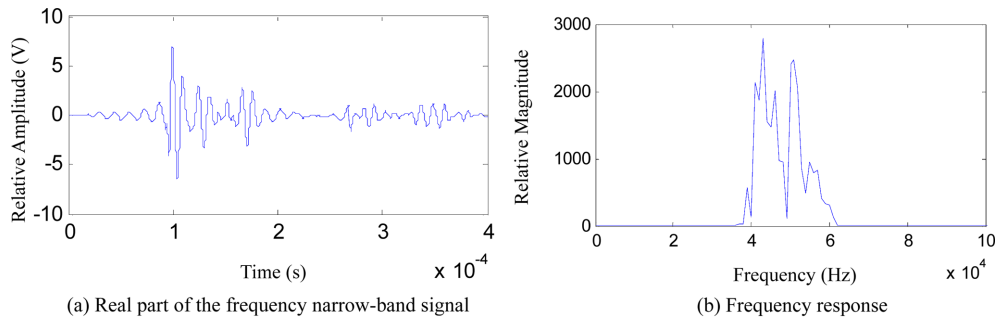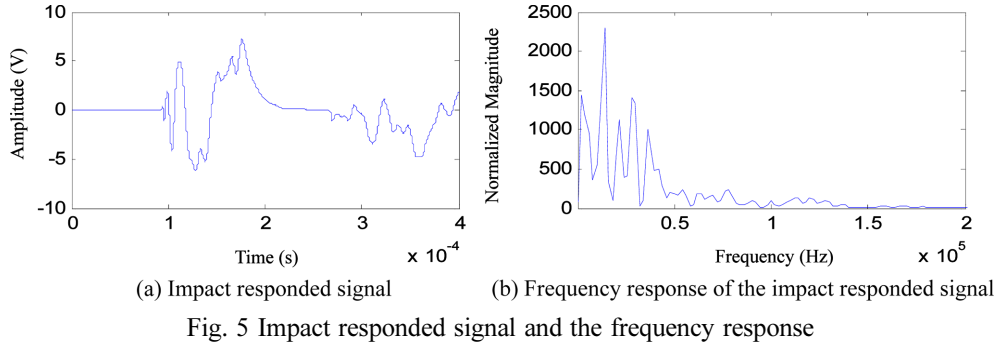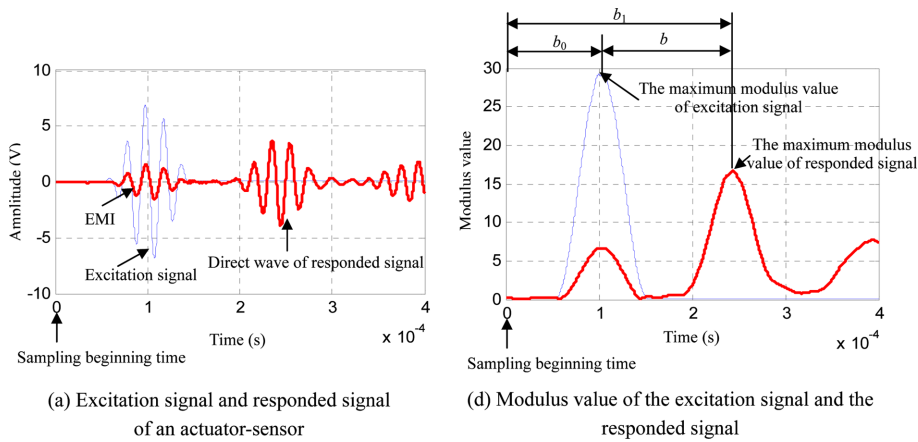Fig. 6 Extracted frequency narrow-band signal, f_c = 50 KHz and f_b = 0.4 f_c

Fig. 5 gives out a typical impact responded signal of a PZT sensor and its frequency response. The sampling rate is 10 MHz. It shows that most of the signal energy distributes in the frequency range of 0 Hz to 60 KHz. Because of this, in this paper, the frequency of 50 KHz is selected to be the center frequency of the frequency narrow-band signals. Depending on the complex Shannon wavelet transform, the frequency narrow-band signal of the center frequency f_c = 50 KHz and the frequency band f_b = 0.4 f_c = 20 KHz is extracted from the impact responded signal. The real part of the signal and the frequency response are shown in Fig. 6.

The continuous complex Shannon wavelet transform is also used to obtain the group velocity in

(a) Excitation signal and responded signal of an actuator-sensor

(d) Modulus value of the excitation signal and the responded signal

Fig. 7 Example of the group velocity measuring

this section. The basic theory can be found in Ding's research (Ding *et al*. 2004). The difference in this paper is that the continuous complex Shannon wavelet transform is used here instead of using the continuous complex Morlet wavelet transform. Fig. 7 gives out an example of the group velocity measured. The excitation signal is a five peak wave signal shown in Fig. 7(a). The modulus value obtained by complex Shannon wavelet transform (f_c = 50 KHz and f_b = $0.4f_c$) of the signals shown in Fig. 7(b).

The time of the maximum modulus value of the excitation signal relative to the sampling beginning time is set to be b_0 and the time when the maximum modulus value of the responded signal happens relative to the sampling beginning time is set to be b_1. The time-of-flight of the signal between the actuator and the sensor can be denoted as $b=b_1-b_0$. Supposing the propagating distance of the Lamb wave from the position of excitation to the sensing is denoted as *Dist*, the group velocity can be represented as

$$C_g = \frac{Dist}{b} \qquad (15)$$

4. Validating experiment

4.1 Experimental set-up and velocity measuring

Evaluation experiments are performed on a composite structure. The dimension of the composite structure is 610 mm long, 600 mm wide and 2.16 mm thick, shown in Fig. 8(a). The composite structure is stacked by 18 single layers. The material property of each layer of the laminated composite structure is shown in Table 1. The thickness of each layer is 0.12 mm and the ply sequences is [45/ 0/-45/90/0/-45/0/-45/0]$_s$. On the composite structure shown in Fig. 8(a). 9 smart layer PZT sensors developed by the authors are arranged and their coordinates are shown in Fig. 8(b). The PZT sensors numbered from 1 to 8 are used to obtain the impact signals. PZT sensor 9 is used to measure the velocities combing with the other 8 PZT sensors. An impact device shown in Fig. 9 is

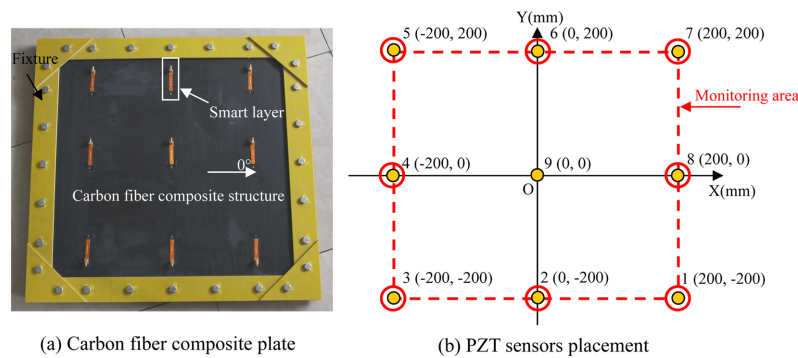(a) Carbon fiber composite plate

(b) PZT sensors placement

Fig. 8 Illustration of carbon fiber composite structure and PZT sensor placement

Table 1 Mechanical parameters of single layer of the carbon fiber composite structure

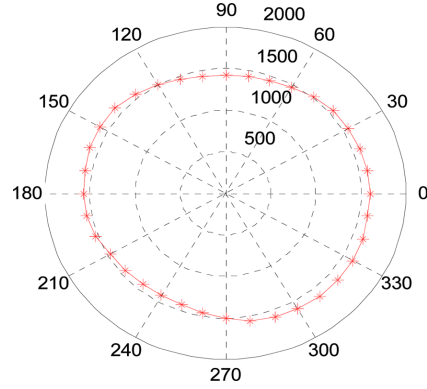| 0º tensile modulus (GPa) E_{11}	90º tensile modulus (GPa) E_{22}	±45ºin-plane shearing modulus (GPa) G_{12}	Main Poisson Ratio μ	Density (kgm^{-3}) ρ
135	8.8	4.47	0.328	1.61×10^3

Fig. 9 The impact device

Fig. 10 The measured group velocity on the composite structure (f_c = 50 KHz)

adopted. The head of the impact device pops out to apply an impact when the trigger is pulled.

The group velocity of the ply direction of 0°, 45°, 90°, 135°, 180°, 225°, 270° and 315° on the structure are measured by the actuator-sensor channels 9-1 to 9-8. The cubic spline interpolation method is adopted to acquire the velocity at each direction of 0° to 360° (10° interval) approximately. Fig. 10 gives out the measured group velocity on the structure.

4.2 Impact imaging results and discussions

To simplify the process of the impact imaging method, the average velocity is adopted. According to the measured velocities of each direction, the average group velocity is 1531 m/s. The search interval Δx and Δy shown in Fig. 3 is set to be 4 mm. The center frequency and the frequency band of the complex Shannon wavelet transform is f_c = 50 KHz and f_b = 0.4 f_c, respectively. Fig. 11(a) gives out a waterfall plot of impact responded signals acquired by the 8 PZT sensors. The frequency narrow-band signals of center frequency 50 KHz and frequency band 20 KHz are extracted from the impact responded signals shown in Fig. 11(b). All the signals are phase modulated depending on the distance from the actual impact to all the PZT sensors and the result is shown in Fig. 12(a). The synthesis signal $|v_s'|$ represented in Eq. (11) is shown in Fig. 12(b).
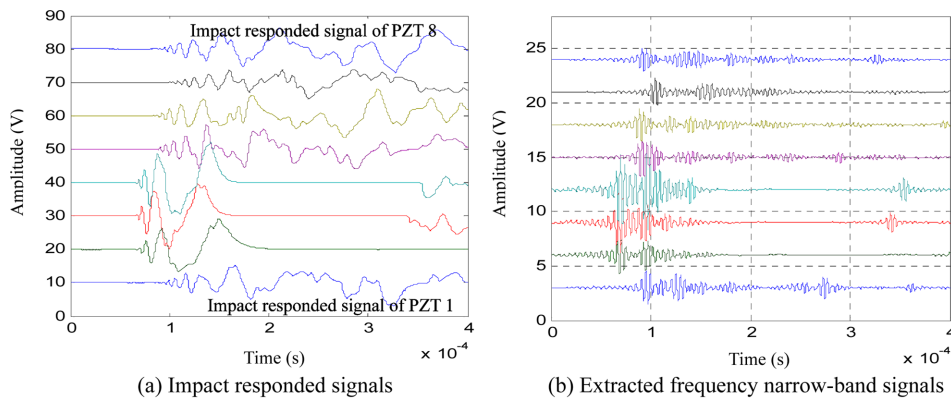

(a) Impact responded signals

(b) Extracted frequency narrow-band signals

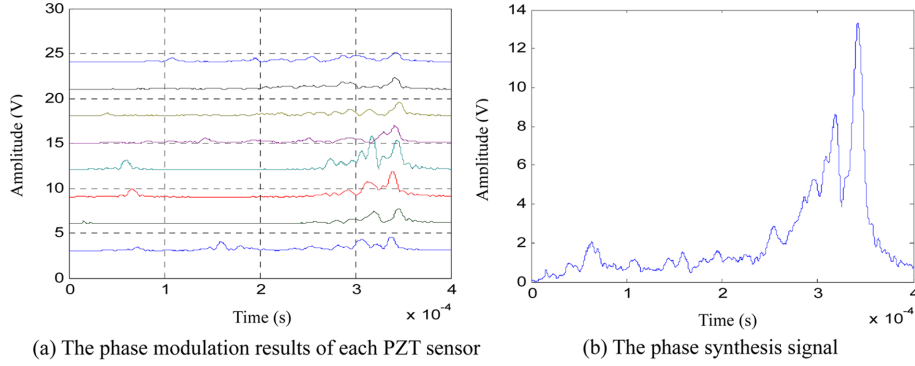Fig. 11 Impact responded signals and the extracted frequency narrow-band signals

(a) The phase modulation results of each PZT sensor   (b) The phase synthesis signal

Fig. 12 Illustration of the phase synthesis at the impact position

(a) The phase modulation results of each PZT sensor   (b) The phase synthesis signal
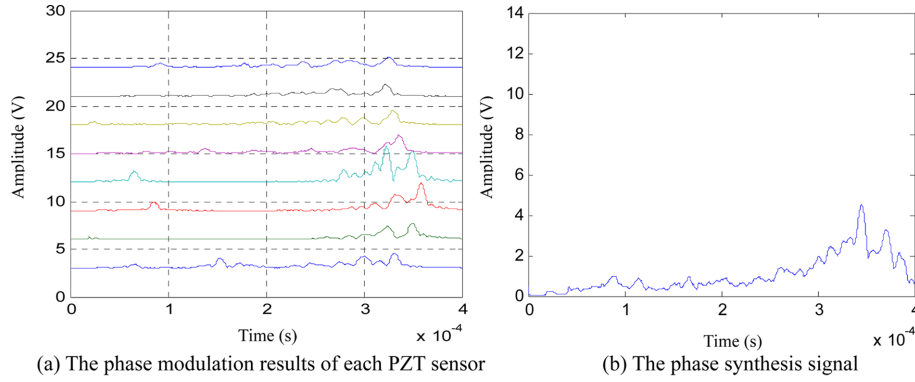
Fig. 13 Phase synthesis result at non-impact position

The phase synthesis result at the position of non-impact is shown in Fig. 13. Comparing it with Fig. 12, the maximum value of the phase synthesis signal at the position of impact is much higher than that of the phase synthesis signal at the position of non-impact.

To highlight the area of higher pixel value, an image normalizing method is adopted in this paper. Normalizing the pixels value in the range of [0, 1] and applying a nonlinear mapping depending on the Eq. (16), the impact monitoring area can be represented as an normalized and mapped maximum modulus value distribution image of the phase synthesis signal. Finally, all mapped pixel values are normalized in the range of [0, 1] again.

$$P \,=\, P^8 \times \tan(P) \tag{16}$$

where P denotes the pixel value, tan denotes the tangent function. Fig. 14 shows the mapping effect of Eq. (16).

Fig. 15 gives out a typical impact imaging result when the impact is at the position (100, 0). It shows that the area of higher pixel value is distributed around the actual impact area. Thus, depending on the impact image, the position of impact can be estimated. This paper uses the coordinate of the point of the maximum pixel value in the impact image to indicate the position of impact. Fig. 16 gives out another six impact imaging results. It shows that the impact imaging method can estimate the position of actual impacts accurately.
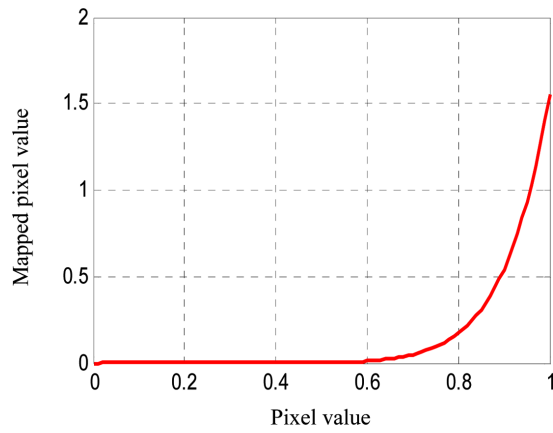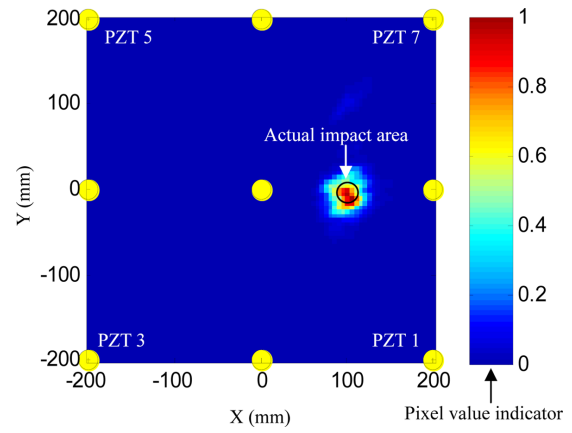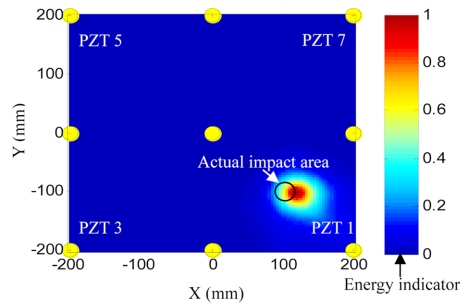
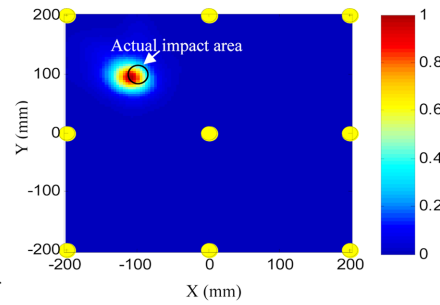Fig. 14 Mapping effect of Eq. (16)
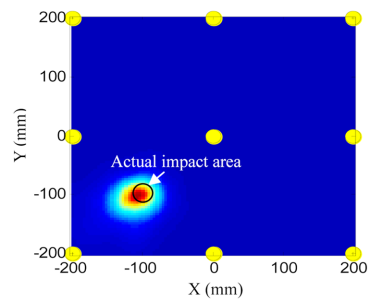

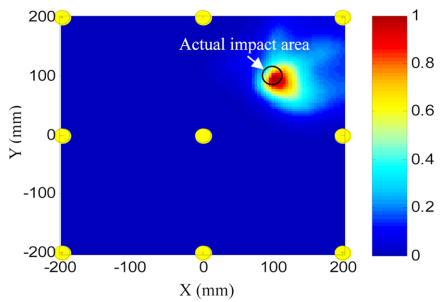Fig. 15 Impact imaging result of the impact 1
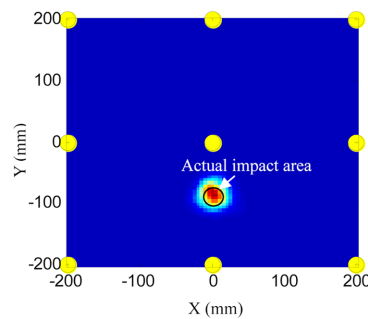

(a) Imaging result of impact 2

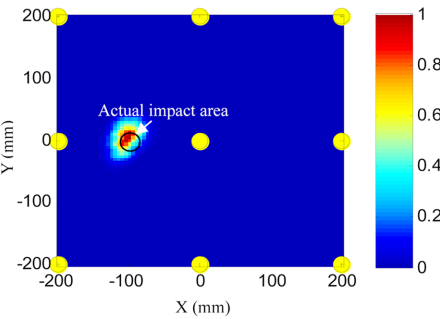(b) Imaging result of impact 3

(c) Imaging result of impact 4

(d) Imaging result of impact 5

(e) Imaging result of impact 6

(f) Imaging result of impact 7

Fig. 16. Impact imaging results on the composite structure in the monitoring area

Table 2 Impact localization results

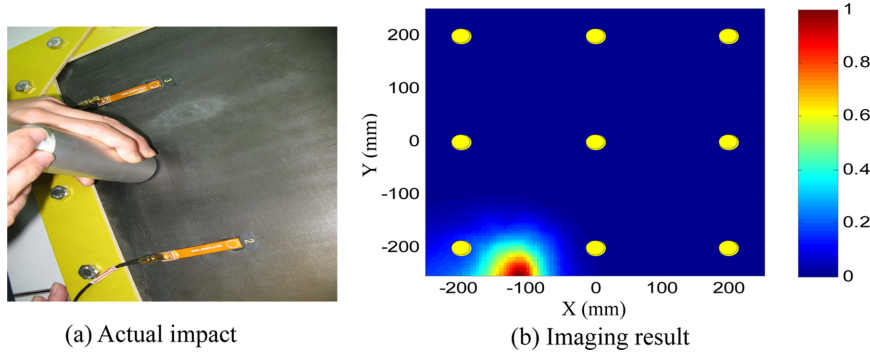| Impact No.	Center coordinate of actual impact (mm, mm)	Estimated center coordinate of impact (mm, mm)	Error (cm)
1	(100, 0)	(105, -10)	1.1
2	(100, -100)	(115, -100)	1.5
3	(-100, 100)	(-110, 95)	1.1
4	(-100, -100)	(-108, -100)	0.8
5	(100, 100)	(104, 96)	0.7
6	(0, -100)	(0, -85)	1.5
7	(-100, 0)	(-100, 10)	1.0

(a) Actual impact　　　　　(b) Imaging result

Fig. 17 Impact imaging result on the composite structure out of the monitoring area

Table 2 gives out the position comparison between the center of actual impacts and the estimated center of impacts depending on the impact images. It indicates that the distance errors of impact localization by the impact imaging method are less than 2.0 cm. Fig. 17 gives out the impact imaging result when the impact happens at the edge area. It shows that even the impact happened at the edge area, the impact position can also be estimated correctly by the imaging method.

Since the average of the group velocity is adopted instead of using the group velocity at different directions on the composite to simply the imaging process. The influence caused by this approximation should be discussed.

The velocity error is defined as

$$Error_{C_g} = \frac{\max\limits_{i=1,...,n} \left| C_{gi} - C_{gaverage} \right|}{C_{gaverage}} \times 100 \tag{17}$$

where $Error_{C_g}$ is the velocity error, $C_{gaverage}$ is the average velocity, C_{gi} denotes the group velocity on the ith direction. In the experiments, the maximum, the minimum and the average group velocities obtained from the specimen are 1626 m/s, 1419 m/s and 1531 m/s, respectively. According to Eq. (17), the maximum error of the group velocity is 7.3%.

To evaluate the influence of the group velocity error, further researches are performed. Different

(a) Impact imaging result of impact 3
($Error_{C_g}$ =25%)

(b) Impact imaging result of impact 3
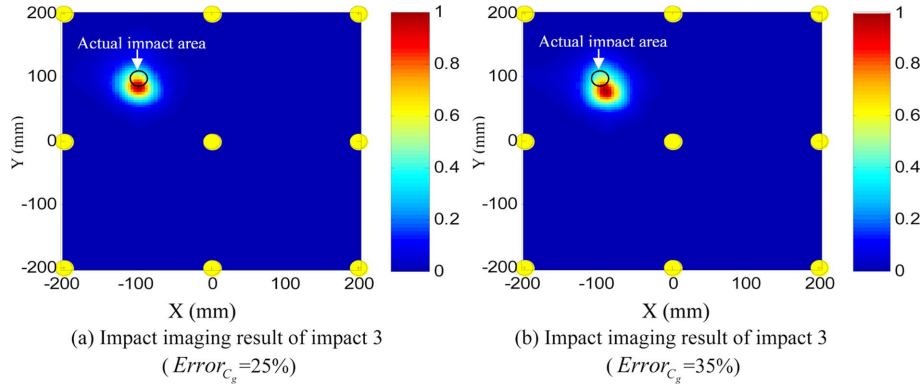($Error_{C_g}$ =35%)

Fig. 18 Impact imaging result of impact 3 when the group velocity error is 25% and 35%

Table 3 Impact localization errors of different group velocity errors

Impact positions	10% velocity error Localization error(cm)	20% velocity error Localization error(cm)	25% velocity error Localization error(cm)	30% velocity error Localization error(cm)	35% velocity error Localization error(cm)
(100, 0)	1.2	1.6	2.2	2.6	3.1
(100, -100)	1.8	2.2	2.7	2.9	3.4
(-100, 100)	1.7	2.2	2.7	3.0	3.5
(-100, -100)	2.0	2.5	2.7	3.2	3.8
(100, 100)	1.4	1.7	2.3	2.8	3.4
(0, -100)	1.9	2.3	2.9	3.4	3.9
(-100, 0)	1.7	2.4	2.8	3.1	3.7

group velocities are used in the impact imaging research and the results are observed. The group velocity are set to have the error of 10%, 20%, 25%, 30% and 35% and applied to the impact imaging of the 7 impact positions. Fig. 18 gives out the imaging results of impact 3 when the group velocity error is 25% and 35%, respectively. They show that the actual impact position can still be estimated correctly, but the localization errors increase. Table 3 calculates the localization errors. It shows that the group velocity errors do influence the imaging. But if the errors of the group velocity are less than 20%, the localization errors are less than 2.5 cm. Considering that even adopting the different group velocities at different directions, still error exists. 20% error of group velocity can be accepted.

In the evaluation experiment, the performance of the presented imaging method under noisy influence is also researched. White noises of signal-to-ratio 10dB and 5dB are added to the impact responded signals respectively to evaluate the image performance under noise. The typical noise containing signals sensed by PZT sensors are shown in Figs. 19(a) and (b). The imaging results are shown in Figs. 19(c) and (d). It can be found that the impact imaging result under 10dB noise is nearly the same as Fig. 16(a). The imaging result under 5dB becomes worse, shown in Fig. 19(d). But the impact position can still be estimated. This means that the presented impact imaging method performs a high antijamming capability.

(a) Impact responded signal (signal-to-ratio is 10dB)   (b) Impact responded signal (signal-to-ratio is 5dB)

(c) Impact imaging result (signal-to-ratio is 10dB)   (d) Impact imaging result (signal-to-ratio is 5dB)
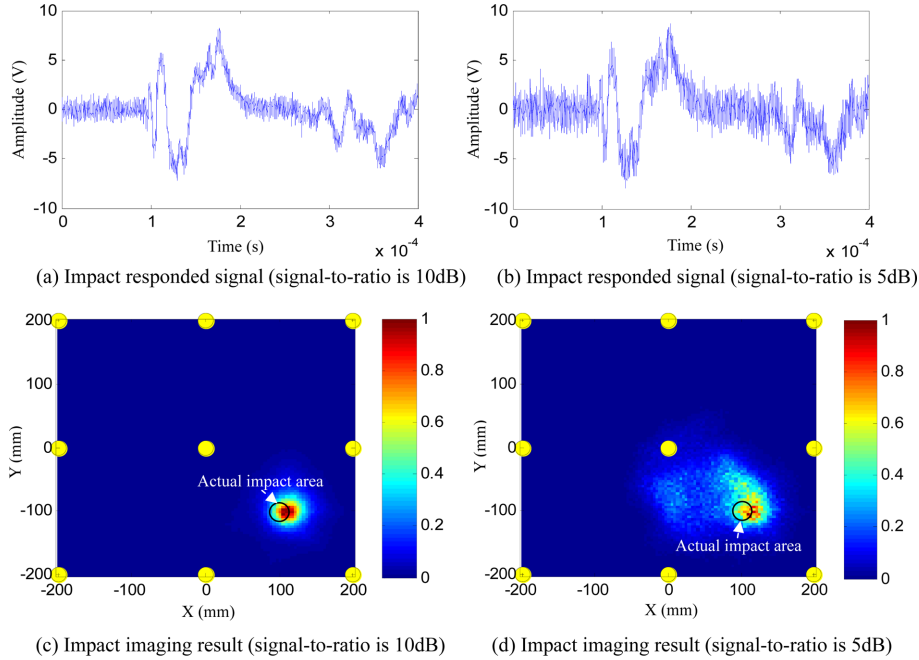
Fig. 19 Impact responded signals with white noises and impact imaging results

5. Conclusions

This paper proposes a PZT sensor array based phase synthesis time reversal focusing and imaging method for impact localization of composite structures on-line. Conventional time reversal focusing process needs the transfer functions of the propagation of the signals on structure to achieve the time reversal focusing in software. In this paper, a phase synthesis method is proposed to achieve the time reversal focusing of impact responded signals. This method does not require any work on the modeling or the measuring of the transfer functions. To be compatible with active structural damage monitoring, PZT sensors are adopted. The complex Shannon wavelet transform is used to extract frequency narrow-band signals from impact responded signals and measure the group velocity of the signals. The impact imaging method avoids training and modeling associated with other techniques and does not need any prior knowledge on structures, except the group velocity.

According to the validating results, localization errors of the impact imaging method are less than 1.5 cm. The impact imaging method using average group velocity can be applied to some complex composite structures if the maximum difference of the group velocity on each direction is in a reasonable range. To some structures of strong anisotropy, the group velocity of each direction must be used. Depending on the time reversal focusing and the complex Shannon wavelet transform, the impact imaging method performs a high antijamming capability.

Further work is ongoing to do the following researches. (1) Studying an image process and position estimation method to determine the position of impact instead of using the maximum pixel value as the impact position in this paper. (2) Validating the impact imaging method on a complex composite structure with many stiffeners and bolt holes and applying the impact imaging method to multi-impact localization.

Acknowledgments

References

Coverley, P.T. and Staszewski, W.J. (2003), "Impact damage location in composite structures using optimized sensor triangulation procedure", *Smart Mater. Struct.*, **12**(5), 795-803.

Chen, C. and Yuan, F.G. (2010), "Impact source identification in finite isotropic plates using a time-reversal method: theoretical study", *Smart Mater. Struct.*, **19**(10), 105028-1-105028-11.

Cai, J., Shi, L., Yuan, S.F. and Shao, Z. (2011), "High spatial resolution imaging for structural health monitoring based on virtual time reversal", *Smart Mater. Struct.*, **20**(5), 055018-1-055018-11.

Ciampa, F. and Meo, M. (2011), "Impact detection in anisotropic materials using a time reversal approach", *Struct. Health Monit.*, 31, doi:10.1177/1475921710395815.

Ding, Y., Reuben, R.L. and Steel, J.A. (2004), "A new method for waveform analysis for estimating AE wave arrival times using wavelet decomposition", *NDT&E Int.*, **37**(4), 279-290.

Efstratios, M.L. and Evangelos, S.D. (2007), "Acoustic emission source location in dispersive media", *Signal Process.*, **87**(12), 3218-3225.

Fink, M. (1992), "Time-Reversal of ultrasonic field--part I: basic principles", *IEEE T. Ultrason. Ferr.*, **39**(5), 555-566.

Fink, M. (1999), "Time-reversed acoustics", *Sci. Am.*, **281**(5), 91-97.

Haywood, J., Coverley, P.T., Staszewski, W.J. and Worden, K. (2005), "An automatic impact monitor for a composite panel employing smart sensor technology", *Smart Mater. Struct.*, **14**(1), 265-271.

Hu, N. and Fukunaga, H. (2007), "An efficient approach for identifying impact force using embedded piezoelectric sensors", *Int. J. Impact Eng.*, **34**(7), 258-1271.

Ing, R.K. and Fink, M. (1996), "Time recompression of dispersive Lamb waves using a time reversal mirror-application to flaw detection in thin plates", *IEEE Ultrasonics Symposium*, **1**, 659-663.

Ing, R.K. and Fink, M. (1998), "Time reversed Lamb waves", *IEEE T. Ultrason. Ferr.*, **45**(4), 1032-1043.

Ing, R.K., Quieffin, N., Cathelinea, S. and Fink, M. (2005), "In solid localization of finger impacts using acoustic time-reversal process", *Appl. Phys. Lett.*, **87**(20), 204104-1-3.

Inoue, H., Harrigan, J.J. and Reid, S.R. (2001), "Review of inverse analysis for indirect measurement of impact force", *Appl. Mech.Rev.*, **54**(6), 503-524.

Jones, R.T., Sirkis, J.S., Friebele, E.J. and Kersey, A.D. (1995), "Location and magnitude of impact detection in composite plates using neural networks", Smart Structures and Materials: Smart Sensing, Processing and Instrumentation, Proc. SPIE 2444, Bellingham,WA: SPIE Optical Engineering Press: 469-80.

Kundu, T., Das, S., Martin, S.A. and Jata, K.V. (2008), "Locating point of impact in anisotropic fiber reinforced composite plates", *Ultrasonics*, **48**(3), 193-201.

Meo, M., Zumpano, G., Piggott, M. and Marengo, G. (2005), "Impact identification on a sandwich plate from wave propagation responses", *Compos. Struct.*, **71**(3-4), 302-306.

Newland, D.E. (1994), "Harmonic and musical wavelets", *Proceedings of the Royal Society of London*, Series A, **444**, 605-620.

Nunez, I. and Negreira, C. (2005), "Efficiency parameters in time reversal acoustics: Applications to dispersive media and multimode wave propagation", *J. Acoust. Soc. Am.*, **117**(3), 1202-1209.

Prada, C. and Fink, M. (1998), "Separation of interfering acoustic scattered signals using the invariants of the time-reversal operator. Application to Lamb waves characterization", *J. Acoust. Soc. Am.*, **104**(2), 801-807.

Park, H.W., Sohn, H., Law, K.H. and Farrar, C.R. (2007), "Time reversal active sensing for health monitoring of a composite plate", *J. Sound Vib.*, **302**(1-2), 50-66.

Park, H.W., Kim, S.B. and Sohn, H. (2009), "Understanding a Time Reversal Process in Lamb Wave Propagation", *Wave Motion*, **46**(7), 451-467.

Ribay, G., Catheline, S., Clorennec, D., Ing, R.K., Quieffin, N. and Fink, M. (2007), "Acoustic impact localization in plates: properties and stability to temperature variation", *IEEE T. Ultrason. Ferr.*, **54**(2), 378-385.

Shin, E.S. (2000), "Real-time recovery of impact force based on finite element analysis", *Comput. Struct.*, **76**(5), 621-627.

Staszewski, W.J., Worden, K. Wardle, R. and Tomlinson, G.R. (2000), "Fail-safe sensor distributions for impact detection in composite materials", *Smart Mater. Struct.*, **9**(3), 298-303.

Staszewski, W.J., Mahzan, S. and Traynor, R. (2009), "Health monitoring of aerospace composite structures-Active and passive approach", *Compos. Sci. Technol.*, **69**(11-12), 1678-1685.

Spanos, P.D. and Kougioumtzoglou, I.A. (2011), "Harmonic wavelets based statistical linearization for response evolutionary power spectrum determination", Probabilistic Engineering Mechanics, article in press, corrected proof.

Teolis, A. (1998), Computational Signal Processing with Wavelets, Birkhauser.

Wang, C., Rose, J.T. and Chang, F.K. (2004), "A synthetic time-reversal imaging method for structural health monitoring", *Smart Mater. Struct.*, **13**(2), 415-423.

Wang, L. and Yuan, F.K. (2005), "Damage identification in a composite plate using pre-stack reverse-time migration technique", *Struct. Health Monit.*, **4**(3), 195-211.

Worden, K. and Staszewski, W.J. (2000), "Impact location and quantification on a composite panel using neural networks and a genetic algorithm", *Strain*, **36**(2), 61-68.

Xu, B. and Giurgiutiu, V. (2007), "Single mode tuning effects on lamb wave time reversal with piezoelectric wafer active sensors for structural health monitoring", *J. Nondestruct. Eval.*, **26**(2-4), 123-134.

BS